On Energy Preserving Consistent Boundary Conditions for the Yee Scheme in 2D

Björn Engquist[†] Jon Häggblad[‡] Olof Runborg[§]

October 21, 2011

Abstract

The Yee scheme is one of the most popular methods for electromagnetic wave propagation. A main advantage is the structured staggered grid, making it simple and efficient on modern computer architectures. A downside to this is the difficulty in approximating oblique boundaries, having to resort to staircase approximations.

In this paper we present a method to improve the boundary treatment in two dimensions by, starting from a staircase approximation, modifying the coefficients of the update stencil so that we can obtain a consistent approximation while preserving the energy conservation, structure and the optimal CFL-condition of the original Yee scheme. We prove this in L_2 and verify it by numerical experiments.

1 Introduction

One of the most common methods for electromagnetic simulations is the Yee scheme, also called the finite-difference time-domain (FDTD) method, introduced in 1966 [33]. It is based on centered explicit differencing on structured staggered grids, making it second order, energy conserving and memory efficient. A major drawback of the method is the difficulty of handling oblique boundaries, which is due to the structured grid. This problem is well-studied [1, 5, 10, 12, 14, 20], and there is a number of approaches to deal with it, e.g., the contour path FDTD [13, 19], the popular locally conformal FDTD methods [3, 4, 35, 23, 36, 37], and hybrid FEM-FDTD methods [21, 16, 32]. There are also many higher order algorithms available [11, 22, 34]. These however, usually suffer from added complexity, slowing or limiting the adoption in the applied fields, such as Electromagnetic Compatibility (EMC). The purpose of this paper is to improve the standard method, rather than to introduce a completely new one.

[†]Department of Mathematics and Institute for Computational Engineering and Sciences, The University of Texas at Austin, 1 University Station C1200, Austin TX 78712, U.S.A. (engquist@ices.utexas.edu)

[‡]Department of Numerical Analysis, CSC, KTH, 100 44 Stockholm, Sweden (jonhagg@csc.kth.se)

[§]Department of Numerical Analysis, CSC, KTH, 100 44 Stockholm, Sweden (olofr@nada.kth.se), and Swedish e-Science Research Center (SeRC)

An approach that was employed by Tornberg and Engquist in [28] is to modify the coefficients of the stencil close to the staircase boundary to create a consistent approximation. This is based on the accurate regularization techniques for wave propagation and discontinuous coefficients developed in [25, 26, 24, 27, 29]. The advantage is that one can keep the structured Yee grid intact, making the method simple as well as easy to implement on modern computer architectures.

In this paper we formulate a new way to modify the coefficients to satisfy the consistency conditions in [28] while at the same time also obtain time-stability, i.e., energy conservation, a property which we show is not present in the original formulation. This makes the method suitable for long simulation times. Furthermore, the modification preserves the CFL-condition of the Yee-scheme, avoiding the need to decrease the timestep and the associated increase in errors. The actual implementation is very simple, since one can post-process the coefficients of a staircase approximation of the boundary before running the simulation. This should make the method easy to incorporate in already existing solvers. Our main contribution in the development of the new algorithm is a rigorous stability analysis in L_2.

2 Background

Consider the transverse electric (TE) and transverse magnetic (TM) modes of Maxwell's equations in two space dimensions. In vacuum the TM mode equation is

$$\begin{aligned} \epsilon \partial_t E_z &= \partial_x H_y - \partial_y H_x, \\ \mu \partial_t H_x &= -\partial_y E_z, \\ \mu \partial_t H_y &= \partial_x E_z, \end{aligned}$$

and the TE mode equation is

$$\begin{aligned} \mu \partial_t H_z &= \partial_y E_x - \partial_x E_y, \\ \epsilon \partial_t E_x &= \partial_y H_z, \\ \epsilon \partial_t E_y &= -\partial_x H_z, \end{aligned}$$

where one assumes no variations along the z-axis. H denotes the magnetic field and E the electric field, while μ and ϵ is the magnetic permeability and electric permittivity, respectively.

For simplicity we will use the acoustic notation,

$$p_t = a(x,y)\left(u_x + v_y\right), \tag{1}$$

$$u_t = b(x,y) p_x, \tag{2}$$

$$v_t = b(x,y) p_y, \tag{3}$$

which is equivalent to the TM and TE mode equations under the substitutions

$$\begin{cases} p = E_z, \\ u = H_y, \\ v = -H_x, \end{cases} \qquad \text{and} \qquad \begin{cases} p = H_z, \\ u = -E_y, \\ v = E_x, \end{cases}$$

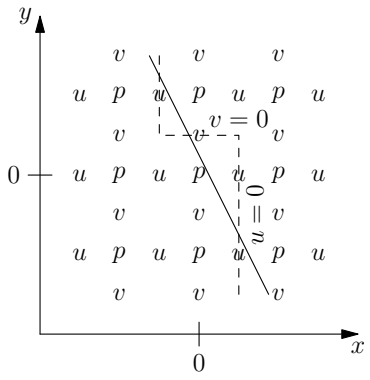

Figure 1: Example of discretization where the computational domain is to the left of the boundary (solid line). The (u, v) components are zero on the dashed staircased boundary.

respectively, together with $a = 1/\epsilon$ and $b = 1/\mu$. Thus we will not use the TE/TM abbreviation any more in this context, and TE will instead refer to a specific generalized discretization later on. The Yee scheme for (1–3) is

$$p^{n+\frac{1}{2}}_{j+\frac{1}{2},l+\frac{1}{2}} = p^{n-\frac{1}{2}}_{j+\frac{1}{2},l+\frac{1}{2}} + \Delta t a_{j+\frac{1}{2},l+\frac{1}{2}} \left(D_{+x} u^n_{j,l+\frac{1}{2}} + D_{+y} v^n_{j+\frac{1}{2},l} \right), \tag{4}$$

$$u^{n+1}_{j,l+\frac{1}{2}} = u^n_{j,l+\frac{1}{2}} + \Delta t b_{j,l+\frac{1}{2}} D_{-x} p^{n+\frac{1}{2}}_{j+\frac{1}{2},l+\frac{1}{2}}, \tag{5}$$

$$v^{n+1}_{j+\frac{1}{2},l} = v^n_{j+\frac{1}{2},l} + \Delta t b_{j+\frac{1}{2},l} D_{-y} p^{n+\frac{1}{2}}_{j+\frac{1}{2},l+\frac{1}{2}}. \tag{6}$$

defined on a grid with $x_j = jh$, $y_l = lh$. Hence $p_{j+\frac{1}{2},l+\frac{1}{2}} \approx p((j+1/2)h, (l+1/2)h)$, $u_{j,l+\frac{1}{2}} \approx u(jh, (l+1/2)h)$ and $v_{j+\frac{1}{2},l} \approx v((j+1/2)h, lh)$. The difference operators are defined by

$$D_{+x} u_{j,l+\frac{1}{2}} = \frac{u_{j+1,l+\frac{1}{2}} - u_{j,l+\frac{1}{2}}}{h_x},$$

$$D_{+y} v_{j+\frac{1}{2},l} = \frac{v_{j+\frac{1}{2},l+1} - v_{j+\frac{1}{2},l}}{h_y},$$

$$D_{-x} p_{j+\frac{1}{2},l+\frac{1}{2}} = \frac{p_{j+\frac{1}{2},l+\frac{1}{2}} - p_{j-\frac{1}{2},l+\frac{1}{2}}}{h_x},$$

$$D_{-y} p_{j+\frac{1}{2},l+\frac{1}{2}} = \frac{p_{j+\frac{1}{2},l+\frac{1}{2}} - p_{j+\frac{1}{2},l-\frac{1}{2}}}{h_y}.$$

The boundary conditions for hard reflections are

$$\hat{\mathbf{n}} \cdot (u, v) = 0, \tag{7}$$

$$\hat{\mathbf{n}} \cdot \nabla p = 0, \tag{8}$$

for $(x, y) \in \partial\Omega$. What was done in [28] was to start from a staircase approximation of the boundary, like in Fig. 1, then use the generalized discretization

$$
\begin{aligned}
\tilde{a}^{\mathrm{E}} \cos\alpha - \tilde{a}^{\mathrm{S}} \sin\alpha &= 0 && \text{(NW)} \\
\tilde{a}^{\mathrm{W}} \cos\alpha + \tilde{a}^{\mathrm{S}} \sin\alpha &= 0 && \text{(NE)} \\
\tilde{a}^{\mathrm{E}} \cos\alpha + \tilde{a}^{\mathrm{N}} \sin\alpha &= 0 && \text{(SW)} \\
\tilde{a}^{\mathrm{W}} \cos\alpha - \tilde{a}^{\mathrm{N}} \sin\alpha &= 0 && \text{(SE)} \\
\tilde{a}^{\mathrm{E}} \cos\alpha + \left(\tilde{a}^{\mathrm{N}} - \tilde{a}^{\mathrm{S}}\right) \sin\alpha &= 0 && \text{(W)} \\
\tilde{a}^{\mathrm{W}} \cos\alpha - \left(\tilde{a}^{\mathrm{N}} - \tilde{a}^{\mathrm{S}}\right) \sin\alpha &= 0 && \text{(E)} \\
\left(\tilde{a}^{\mathrm{E}} - \tilde{a}^{\mathrm{W}}\right) \cos\alpha - \tilde{a}^{\mathrm{S}} \sin\alpha &= 0 && \text{(N)} \\
\left(\tilde{a}^{\mathrm{E}} - \tilde{a}^{\mathrm{W}}\right) \cos\alpha + \tilde{a}^{\mathrm{N}} \sin\alpha &= 0 && \text{(S)}
\end{aligned}
$$

Table 1: Summary of the consistency conditions. The labeling corresponds to the one defined in Fig. 2.

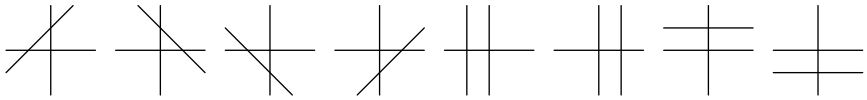

(a) NW (b) NE (c) SW (d) SE (e) W (f) E (g) N (h) S

Figure 2: The eight different cases for how the boundary can intersect the update stencil for p.

$$
(9) \qquad a(u_x + v_y)\Big|_{\substack{j+1/2 \\ l+1/2}} \approx \frac{a_{j+1/2,l+1/2}}{h} \left(\tilde{a}^{\mathrm{E}} u^{\mathrm{E}} - \tilde{a}^{\mathrm{W}} u^{\mathrm{W}} + \tilde{a}^{\mathrm{N}} v^{\mathrm{N}} - \tilde{a}^{\mathrm{S}} v^{\mathrm{S}}\right),
$$

where the new coefficients $\tilde{a}^{\mathrm{E}}, \tilde{a}^{\mathrm{W}}, \tilde{a}^{\mathrm{N}}, \tilde{a}^{\mathrm{S}}$ are set to satisfy the *consistency conditions* in Table 1, which arise from the boundary condition (7). We will refer to this class of methods as *Tornberg–Engquist* (TE) type modifications*. Doing this removes the lowest order error term in the spatial discretization of the boundary, which is $\tau_{\mathrm{Yee}} = \mathcal{O}(1/h)$, thus obtaining $\tau_{\mathrm{TE}} = \mathcal{O}(1)$ and the error of the full solution becomes $\Delta t \tau_{\mathrm{TE}} = \mathcal{O}(h)$, instead of $\Delta t \tau_{\mathrm{Yee}} = \mathcal{O}(1)$.

With regards to the question of stability. There is no proof of this, but numerical experiments indicate that the strategy for modifying the coefficients in [28] yield an error growth proportional to Δt at every timestep. This means we have a stability bound of the form

$$
\|p^{n-1/2}\|_h + \|u^n\|_h + \|v^n\|_h \leq C e^{\alpha t_n} \left(\|p^{-1/2}\|_h + \|u^0\|_h + \|v^0\|_h\right), \quad \forall n > 0,
$$

meaning the method, while numerically stable, is not energy preserving. See Fig. 3 for an example. Preferably we would like to have a consistent method with $\alpha = 0$,

$$
(10) \quad \|p^{n-1/2}\|_h + \|u^n\|_h + \|v^n\|_h \leq C \left(\|p^{-1/2}\|_h + \|u^0\|_h + \|v^0\|_h\right), \quad \forall n > 0,
$$

making it suitable for long simulation times. Note that C is independent of n. This stronger form of stability (10) has many names in the literature, but we will use the term *time-stability* as defined by [8, 30, 31, 2]. This is also called asympotic stability or strict stability [6, 15, 18]. See [9, 7] for more on GKS stability theory.

*Note that TE will never refer to the transverse electric field from here on.

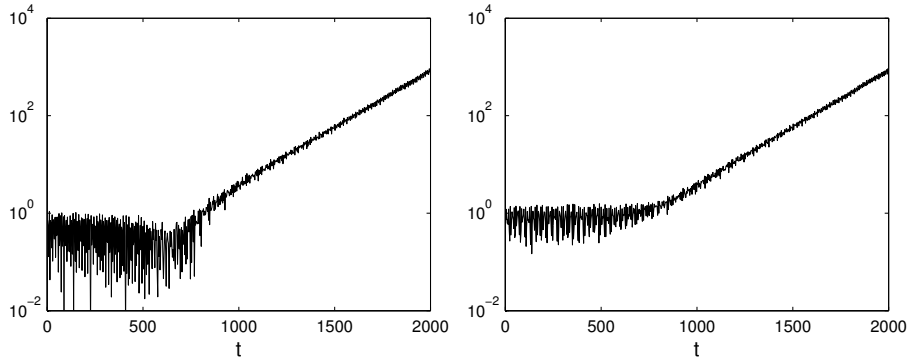

(a) $\|p^{n-1/2}\|_h$ (b) $\|\mathbf{u}^n\|_h$

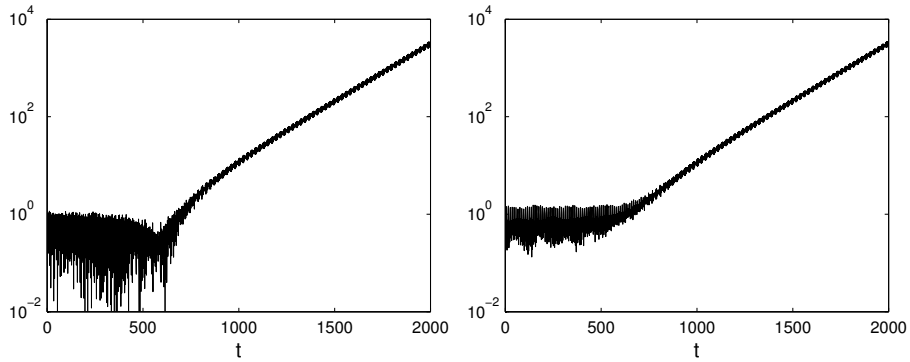

(c) $\|p^{n-1/2}\|_h$ (d) $\|\mathbf{u}^n\|_h$

Figure 3: For long times we observe exponential growth of the solution that is independent of the number of time steps, indicating that we still have stability, albeit not time-stability. We initialize the grid with uniformly random data to excite all frequencies representable on the grid. Parameters of the problem are $a = b = -1$, $N = 64$, $\lambda = \Delta t/h = 0.3$, with a boundary defined by $y = (x - \bar{x}) \tan\alpha + \sqrt{\epsilon_{\text{mach}}}$ for $\bar{x} = \pi(1 - \sqrt{3} + \sqrt{2}/100)/2$ and $\alpha = \pi/6$. In (c) and (d) we divide the time step by 3, yet we still observe that the growth to start approximately at the same physical time. Note that for the velocity field $\mathbf{u} = (u, v)$ we use the Euclidean norm.

3 A class of time-stable discretizations

To obtain a time-stable modification of the coefficients along the boundary we consider a general numerical scheme, which we will later adapt such that it reduces to the standard Yee scheme in the internal domain and at the same time satisfies the consistency conditions on the boundary. Thus let

$$
\begin{aligned}
p_{j+\frac{1}{2},l+\frac{1}{2}}^{n+\frac{1}{2}} = p_{j+\frac{1}{2},l+\frac{1}{2}}^{n-\frac{1}{2}} &+ \Delta t a_{j+\frac{1}{2},l+\frac{1}{2}}^{(1)} D_{+x}\left(\alpha_{j,l+\frac{1}{2}}^{(1)} u_{j,l+\frac{1}{2}}^{n}\right) \\
&+ \Delta t a_{j+\frac{1}{2},l+\frac{1}{2}}^{(2)} D_{+y}\left(\alpha_{j+\frac{1}{2},l}^{(2)} v_{j+\frac{1}{2},l}^{n}\right),
\end{aligned} \tag{11}
$$

$$
u_{j,l+\frac{1}{2}}^{n+1} = u_{j,l+\frac{1}{2}}^{n} + \Delta t b_{j,l+\frac{1}{2}}^{(1)} D_{-x}\left(\beta_{j+\frac{1}{2},l+\frac{1}{2}}^{(1)} p_{j+\frac{1}{2},l+\frac{1}{2}}^{n+\frac{1}{2}}\right), \tag{12}
$$

$$
v_{j+\frac{1}{2},l}^{n+1} = v_{j+\frac{1}{2},l}^{n} + \Delta t b_{j+\frac{1}{2},l}^{(2)} D_{-y}\left(\beta_{j+\frac{1}{2},l+\frac{1}{2}}^{(2)} p_{j+\frac{1}{2},l+\frac{1}{2}}^{n+\frac{1}{2}}\right), \tag{13}
$$

where we assume zero outer boundary data (homogeneous Dirichlet conditions). The coefficients are assumed to be bounded from above and below. We also introduce

$$
\begin{aligned}
c_{j+\frac{1}{2},l+\frac{1}{2}}^{(1)} &= \frac{1}{2}\sqrt{a_{\substack{j+\frac{1}{2}\\ l+\frac{1}{2}}}^{(1)} \beta_{\substack{j+\frac{1}{2}\\ l+\frac{1}{2}}}^{(1)}}\left(\sqrt{\alpha_{\substack{j\\ l+\frac{1}{2}}}^{(1)} b_{\substack{j\\ l+\frac{1}{2}}}^{(1)}} + \sqrt{\alpha_{\substack{j+1\\ l+\frac{1}{2}}}^{(1)} b_{\substack{j+1\\ l+\frac{1}{2}}}^{(1)}}\right), \\
c_{j,l+\frac{1}{2}}^{(1)} &= \frac{1}{2}\left(\sqrt{a_{\substack{j+\frac{1}{2}\\ l+\frac{1}{2}}}^{(1)} \beta_{\substack{j+\frac{1}{2}\\ l+\frac{1}{2}}}^{(1)}} + \sqrt{a_{\substack{j-\frac{1}{2}\\ l+\frac{1}{2}}}^{(1)} \beta_{\substack{j-\frac{1}{2}\\ l+\frac{1}{2}}}^{(1)}}\right)\sqrt{\alpha_{\substack{j\\ l+\frac{1}{2}}}^{(1)} b_{\substack{j\\ l+\frac{1}{2}}}^{(1)}}, \\
c_{j+\frac{1}{2},l+\frac{1}{2}}^{(2)} &= \frac{1}{2}\sqrt{a_{\substack{j+\frac{1}{2}\\ l+\frac{1}{2}}}^{(2)} \beta_{\substack{j+\frac{1}{2}\\ l+\frac{1}{2}}}^{(2)}}\left(\sqrt{\alpha_{\substack{j+\frac{1}{2}\\ l}}^{(2)} b_{\substack{j+\frac{1}{2}\\ l}}^{(2)}} + \sqrt{\alpha_{\substack{j+\frac{1}{2}\\ l+1}}^{(2)} b_{\substack{j+\frac{1}{2}\\ l+1}}^{(2)}}\right), \\
c_{j+\frac{1}{2},l}^{(2)} &= \frac{1}{2}\left(\sqrt{a_{\substack{j+\frac{1}{2}\\ l-\frac{1}{2}}}^{(2)} \beta_{\substack{j+\frac{1}{2}\\ l-\frac{1}{2}}}^{(2)}} + \sqrt{a_{\substack{j+\frac{1}{2}\\ l+\frac{1}{2}}}^{(2)} \beta_{\substack{j+\frac{1}{2}\\ l+\frac{1}{2}}}^{(2)}}\right)\sqrt{\alpha_{\substack{j+\frac{1}{2}\\ l}}^{(2)} b_{\substack{j+\frac{1}{2}\\ l}}^{(2)}},
\end{aligned}
$$

and the discrete L_2-norms generated by the inner products

$$
\langle p^{(1)}, p^{(2)} \rangle_h = \sum_{j,l \in \Omega_N^p} p_{j+\frac{1}{2},l+\frac{1}{2}}^{(1)} p_{j+\frac{1}{2},l+\frac{1}{2}}^{(2)} h^2, \tag{14}
$$

$$
\langle u^{(1)}, u^{(2)} \rangle_h = \sum_{j,l \in \Omega_N^u} u_{j,l+\frac{1}{2}}^{(1)} u_{j,l+\frac{1}{2}}^{(2)} h^2, \tag{15}
$$

$$
\langle v^{(1)}, v^{(2)} \rangle_h = \sum_{j,l \in \Omega_N^v} v_{j+\frac{1}{2},l}^{(1)} v_{j+\frac{1}{2},l}^{(2)} h^2. \tag{16}
$$

The superscripts designate different grid functions. Although we employ the same notation for all three inner products, which one is used should be clear from which grid functions they are applied on. Here we use the sets Ω_N^p, Ω_N^u and Ω_N^v, which contains the indices corresponding to field points inside the internal domain, for respective variable.

Theorem 3.1 (Stability)**.** *The discretization (11–13) is time-stable, i.e.,*

$$
\|p^{n-\frac{1}{2}}\|_h + \|u^n\|_h + \|v^n\|_h \leq C\left(\|p^{-\frac{1}{2}}\|_h + \|u^0\|_h + \|v^0\|_h\right),
$$

with C independent of n, if

$$\frac{\beta^{(1)}_{j+\frac{1}{2},l+\frac{1}{2}}}{a^{(1)}_{j+\frac{1}{2},l+\frac{1}{2}}} = \frac{\beta^{(2)}_{j+\frac{1}{2},l+\frac{1}{2}}}{a^{(2)}_{j+\frac{1}{2},l+\frac{1}{2}}}, \qquad \forall j,l \in \Omega^p_N, \tag{17}$$

and

$$\lambda \max_{i\in\{1,2\}} \max_{j,l} c^{(i)} \leq \frac{1-\delta}{\sqrt{2}}, \qquad \delta > 0, \tag{18}$$

are satisfied.

The proof follows from two Lemmas. First we need to define two discrete quantities, N_h and E_h, by

$$N_h(p^{n-\frac{1}{2}}, u^n, v^n) = \left\| \sqrt{\frac{\beta^{(1)}}{a^{(1)}}} p^{n-\frac{1}{2}} \right\|_h^2 + \left\| \sqrt{\frac{\alpha^{(1)}}{b^{(1)}}} u^n \right\|_h^2 + \left\| \sqrt{\frac{\alpha^{(2)}}{b^{(2)}}} v^n \right\|_h^2,$$

$$\begin{aligned} E_h(p^{n-\frac{1}{2}}, u^n, v^n) = N_h &- \Delta t \left\langle \alpha^{(1)} u^n, D_{-x}\left(\beta^{(1)} p^{n-\frac{1}{2}}\right) \right\rangle_h \\ &- \Delta t \left\langle \alpha^{(2)} v^n, D_{-x}\left(\beta^{(2)} p^{n-\frac{1}{2}}\right) \right\rangle_h \end{aligned} \tag{19}$$

Lemma 3.1. *For $a^{(i)}\beta^{(i)} > 0$, $\alpha^{(i)} b^{(i)} > 0$, $i = 1, 2$, the discretization (11–13) conserves the quantity E_h, i.e.,*

$$E_h(p^{n-\frac{1}{2}}, u^n, v^n) = E_h(p^{-\frac{1}{2}}, u^0, v^0), \qquad \forall n > 0,$$

if (17) *is satisfied.*

Proof. Expanding (11–13) according to

$$\begin{aligned} p^{n+\frac{1}{2}}_{j+\frac{1}{2},l+\frac{1}{2}} &= p^{n-\frac{1}{2}}_{j+\frac{1}{2},l+\frac{1}{2}} + \Delta t \frac{a^{(1)}_{j+\frac{1}{2},l+\frac{1}{2}}}{\beta^{(1)}_{j+\frac{1}{2},l+\frac{1}{2}}} \beta^{(1)}_{j+\frac{1}{2},l+\frac{1}{2}} D_{+x}\left(\alpha^{(1)}_{j,l+\frac{1}{2}} u^n_{j,l+\frac{1}{2}}\right) \\ &\quad + \Delta t \frac{a^{(2)}_{j+\frac{1}{2},l+\frac{1}{2}}}{\beta^{(2)}_{j+\frac{1}{2},l+\frac{1}{2}}} \beta^{(2)}_{j+\frac{1}{2},l+\frac{1}{2}} D_{+y}\left(\alpha^{(2)}_{j+\frac{1}{2},l} v^n_{j+\frac{1}{2},l}\right), \\ u^{n+1}_{j,l+\frac{1}{2}} &= u^n_{j,l+\frac{1}{2}} + \Delta t \frac{b^{(1)}_{j,l+\frac{1}{2}}}{\alpha^{(1)}_{j,l+\frac{1}{2}}} \alpha^{(1)}_{j,l+\frac{1}{2}} D_{-x}\left(\beta^{(1)}_{j+\frac{1}{2},l+\frac{1}{2}} p^{n+\frac{1}{2}}_{j+\frac{1}{2},l+\frac{1}{2}}\right), \\ v^{n+1}_{j+\frac{1}{2},l} &= v^n_{j+\frac{1}{2},l} + \Delta t \frac{b^{(2)}_{j+\frac{1}{2},l}}{\alpha^{(2)}_{j+\frac{1}{2},l}} \alpha^{(2)}_{j+\frac{1}{2},l} D_{-y}\left(\beta^{(2)}_{j+\frac{1}{2},l+\frac{1}{2}} p^{n+\frac{1}{2}}_{j+\frac{1}{2},l+\frac{1}{2}}\right), \end{aligned}$$

and then divide away the coefficient as well as multiplying with the conjugate, we get

$$\begin{aligned} \frac{\beta^{(1)}_{j+\frac{1}{2},l+\frac{1}{2}}}{a^{(1)}_{j+\frac{1}{2},l+\frac{1}{2}}} &\left[\left(p^{n+\frac{1}{2}}_{j+\frac{1}{2},l+\frac{1}{2}}\right)^2 - \left(p^{n-\frac{1}{2}}_{j+\frac{1}{2},l+\frac{1}{2}}\right)^2 \right] = \Delta t \Bigg(\beta^{(1)}_{j+\frac{1}{2},l+\frac{1}{2}} D_{+x}\left(\alpha^{(1)}_{j,l+\frac{1}{2}} u^n_{j,l+\frac{1}{2}}\right) \\ &+ \beta^{(2)}_{j+\frac{1}{2},l+\frac{1}{2}} D_{+y}\left(\alpha^{(2)}_{j+\frac{1}{2},l} v^n_{j+\frac{1}{2},l}\right) \Bigg) \left(p^{n+\frac{1}{2}}_{j+\frac{1}{2},l+\frac{1}{2}} + p^{n-\frac{1}{2}}_{j+\frac{1}{2},l+\frac{1}{2}}\right), \end{aligned} \tag{20}$$

$$\frac{\alpha^{(1)}_{j,l+\frac{1}{2}}}{b^{(1)}_{j,l+\frac{1}{2}}}\left[\left(u^{n+1}_{j,l+\frac{1}{2}}\right)^2-\left(u^{n}_{j,l+\frac{1}{2}}\right)^2\right]$$
$$=\Delta t\alpha^{(1)}_{j,l+\frac{1}{2}}D_{-x}\left(\beta^{(1)}_{j+\frac{1}{2},l+\frac{1}{2}}p^{n+\frac{1}{2}}_{j+\frac{1}{2},l+\frac{1}{2}}\right)\left(u^{n+1}_{j,l+\frac{1}{2}}+u^{n}_{j,l+\frac{1}{2}}\right),$$

$$\frac{\alpha^{(2)}_{j+\frac{1}{2},l}}{b^{(2)}_{j+\frac{1}{2},l}}\left[\left(v^{n+1}_{j+\frac{1}{2},l}\right)^2-\left(v^{n}_{j+\frac{1}{2},l}\right)^2\right]$$
$$=\Delta t\alpha^{(2)}_{j+\frac{1}{2},l}D_{-y}\left(\beta^{(2)}_{j+\frac{1}{2},l+\frac{1}{2}}p^{n+\frac{1}{2}}_{j+\frac{1}{2},l+\frac{1}{2}}\right)\left(v^{n+1}_{j+\frac{1}{2},l}+v^{n}_{j+\frac{1}{2},l}\right).$$

Hence summing gives us

$$\left\|\sqrt{\frac{\beta^{(1)}}{a^{(1)}}}p^{n+\frac{1}{2}}\right\|_h^2=\left\|\sqrt{\frac{\beta^{(1)}}{a^{(1)}}}p^{n-\frac{1}{2}}\right\|_h^2 + \Delta t\left\langle\beta^{(1)}D_{+x}\left(\alpha^{(1)}u^n\right)+\beta^{(2)}D_{+y}\left(\alpha^{(2)}v^n\right),p^{n+\frac{1}{2}}+p^{n-\frac{1}{2}}\right\rangle_h, \tag{21}$$

$$\left\|\sqrt{\frac{\alpha^{(1)}}{b^{(1)}}}u^{n+1}\right\|_h^2=\left\|\sqrt{\frac{\alpha^{(1)}}{b^{(1)}}}u^{n}\right\|_h^2+\Delta t\left\langle\alpha^{(1)}D_{-x}\left(\beta^{(1)}p^{n+\frac{1}{2}}\right),u^{n+1}+u^n\right\rangle_h, \tag{22}$$

$$\left\|\sqrt{\frac{\alpha^{(2)}}{b^{(2)}}}v^{n+1}\right\|_h^2=\left\|\sqrt{\frac{\alpha^{(2)}}{b^{(2)}}}v^{n}\right\|_h^2+\Delta t\left\langle\alpha^{(2)}D_{-y}\left(\beta^{(2)}p^{n+\frac{1}{2}}\right),v^{n+1}+v^n\right\rangle_h. \tag{23}$$

Now we need to find the form of the conserved quantity. To do this we first sum the three terms involving inner-products in (21–23) to get

$$\begin{aligned}&\Delta t\left\langle\beta^{(1)}D_{+x}\left(\alpha^{(1)}u^n\right)+\beta^{(2)}D_{+y}\left(\alpha^{(2)}v^n\right),p^{n+\frac{1}{2}}+p^{n-\frac{1}{2}}\right\rangle_h\\ &\quad+\Delta t\left\langle\alpha^{(1)}D_{-x}\left(\beta^{(1)}p^{n+\frac{1}{2}}\right),u^{n+1}+u^n\right\rangle_h\\ &\quad+\Delta t\left\langle\alpha^{(2)}D_{-y}\left(\beta^{(2)}p^{n+\frac{1}{2}}\right),v^{n+1}+v^n\right\rangle_h.\end{aligned}$$

Since both u and v are zero on the internal and external boundaries, we have the identities

$$\begin{aligned}\langle D_{+x}u,v\rangle_h&=-\langle u,D_{-x}v\rangle_h,\\ \langle D_{+y}u,v\rangle_h&=-\langle u,D_{-y}v\rangle_h,\end{aligned}$$

and we can rewrite (3) to

$$\begin{aligned}&-\Delta t\left\langle\alpha^{(1)}u^n,D_{-x}\left(\beta^{(1)}p^{n+\frac{1}{2}}\right)\right\rangle_h-\Delta t\left\langle\alpha^{(2)}v^n,D_{-x}\left(\beta^{(2)}p^{n+\frac{1}{2}}\right)\right\rangle_h\\ &\quad-\Delta t\left\langle\alpha^{(1)}u^n,D_{-x}\left(\beta^{(1)}p^{n-\frac{1}{2}}\right)\right\rangle_h-\Delta t\left\langle\alpha^{(2)}v^n,D_{-x}\left(\beta^{(2)}p^{n-\frac{1}{2}}\right)\right\rangle_h\\ &+\Delta t\left\langle\alpha^{(1)}u^{n+1},D_{-x}\left(\beta^{(1)}p^{n+\frac{1}{2}}\right)\right\rangle_h+\Delta t\left\langle\alpha^{(2)}v^{n+1},D_{-x}\left(\beta^{(2)}p^{n+\frac{1}{2}}\right)\right\rangle_h\\ &\quad+\Delta t\left\langle\alpha^{(1)}u^{n},D_{-x}\left(\beta^{(1)}p^{n+\frac{1}{2}}\right)\right\rangle_h+\Delta t\left\langle\alpha^{(2)}v^{n},D_{-x}\left(\beta^{(2)}p^{n+\frac{1}{2}}\right)\right\rangle_h\end{aligned}$$

which simplifies to

$$
\begin{aligned}
(24)\quad & -\Delta t\left\langle \alpha^{(1)}u^n, D_{-x}\left(\beta^{(1)}p^{n-\frac{1}{2}}\right)\right\rangle_h - \Delta t\left\langle \alpha^{(2)}v^n, D_{-x}\left(\beta^{(2)}p^{n-\frac{1}{2}}\right)\right\rangle_h \\
& + \Delta t\left\langle \alpha^{(1)}u^{n+1}, D_{-x}\left(\beta^{(1)}p^{n+\frac{1}{2}}\right)\right\rangle_h + \Delta t\left\langle \alpha^{(2)}v^{n+1}, D_{-x}\left(\beta^{(2)}p^{n+\frac{1}{2}}\right)\right\rangle_h .
\end{aligned}
$$

We see that we get two identical expression with opposite sign and different time levels n. Hence, summing (21–23) and using (24), we obtain $E_h(p^{n+\frac{1}{2}}, u^{n+1}, v^{n+1}) = E_h(p^{n-\frac{1}{2}}, u^n, v^n)$, and the conservation of E_h follows. □

Now we will derive the condition necessary for E_h to define an energy, more precisely a norm that is equivalent with N_h uniformly in h.

Lemma 3.2. *Suppose* (18) *is satisfied, then*

$$
\delta N_h \le E_h \le (2-\delta)N_h. \tag{25}
$$

Proof. We need to bound the second part of (19). The first of these two terms expands to

$$
\begin{aligned}
(26)\quad & \Delta t\left|\left\langle \alpha^{(1)}u^n, D_{-x}\left(\beta^{(1)}p^{n-\frac{1}{2}}\right)\right\rangle_h\right| \\
& \qquad = \left|\sum_{j,l}\lambda\left(\beta^{(1)}_{j+\frac{1}{2},l+\frac{1}{2}}p^{n-\frac{1}{2}}_{j+\frac{1}{2},l+\frac{1}{2}} - \beta^{(1)}_{j-\frac{1}{2},l+\frac{1}{2}}p^{n-\frac{1}{2}}_{j-\frac{1}{2},l+\frac{1}{2}}\right)\alpha^{(1)}_{j,l+\frac{1}{2}}u^n_{j,l+\frac{1}{2}}h^2\right|.
\end{aligned}
$$

Thus using the triangle inequality as well as

$$
\nu\gamma xy \le \frac{1}{2}\left(\frac{1}{\sqrt{2}}\nu^2x^2 + \sqrt{2}\gamma^2y^2\right),
$$

we can bound (26) by

$$
\begin{aligned}
& \le \frac{\lambda}{2}\sum_{j,l}\sqrt{a^{(1)}_{\substack{j+\frac{1}{2}\\ l+\frac{1}{2}}}\beta^{(1)}_{\substack{j+\frac{1}{2}\\ l+\frac{1}{2}}}\alpha^{(1)}_{\substack{j\\ l+\frac{1}{2}}}b^{(1)}_{\substack{j\\ l+\frac{1}{2}}}}\left(\frac{1}{\sqrt{2}}\left|\sqrt{\frac{\beta^{(1)}}{a^{(1)}}}p^{n-\frac{1}{2}}\right|^2_{\substack{j+\frac{1}{2}\\ l+\frac{1}{2}}} + \sqrt{2}\left|\sqrt{\frac{\alpha^{(1)}}{b^{(1)}}}u^n\right|^2_{\substack{j\\ l+\frac{1}{2}}}\right)h^2 \\
& \quad + \sqrt{a^{(1)}_{\substack{j-\frac{1}{2}\\ l+\frac{1}{2}}}\beta^{(1)}_{\substack{j-\frac{1}{2}\\ l+\frac{1}{2}}}\alpha^{(1)}_{\substack{j\\ l+\frac{1}{2}}}b^{(1)}_{\substack{j\\ l+\frac{1}{2}}}}\left(\frac{1}{\sqrt{2}}\left|\sqrt{\frac{\beta^{(1)}}{a^{(1)}}}p^{n-\frac{1}{2}}\right|^2_{\substack{j-\frac{1}{2}\\ l+\frac{1}{2}}} + \sqrt{2}\left|\sqrt{\frac{\alpha^{(1)}}{b^{(1)}}}u^n\right|^2_{\substack{j\\ l+\frac{1}{2}}}\right)h^2 \\
& = \lambda\sum_{j,l}\overbrace{\frac{1}{2}\sqrt{a^{(1)}_{\substack{j+\frac{1}{2}\\ l+\frac{1}{2}}}\beta^{(1)}_{\substack{j+\frac{1}{2}\\ l+\frac{1}{2}}}}\left(\sqrt{\alpha^{(1)}_{\substack{j\\ l+\frac{1}{2}}}b^{(1)}_{\substack{j\\ l+\frac{1}{2}}}} + \sqrt{\alpha^{(1)}_{\substack{j+1\\ l+\frac{1}{2}}}b^{(1)}_{\substack{j+1\\ l+\frac{1}{2}}}}\right)}^{c^{(1)}_{j+1/2,l+1/2}}\frac{1}{\sqrt{2}}\left|\sqrt{\frac{\beta^{(1)}}{a^{(1)}}}p^{n-\frac{1}{2}}\right|^2_{\substack{j+\frac{1}{2}\\ l+\frac{1}{2}}} \\
& \quad + \underbrace{\frac{1}{2}\left(\sqrt{a^{(1)}_{\substack{j+\frac{1}{2}\\ l+\frac{1}{2}}}\beta^{(1)}_{\substack{j+\frac{1}{2}\\ l+\frac{1}{2}}}} + \sqrt{a^{(1)}_{\substack{j-\frac{1}{2}\\ l+\frac{1}{2}}}\beta^{(1)}_{\substack{j-\frac{1}{2}\\ l+\frac{1}{2}}}}\right)\sqrt{\alpha^{(1)}_{\substack{j\\ l+\frac{1}{2}}}b^{(1)}_{\substack{j\\ l+\frac{1}{2}}}}}_{c^{(1)}_{j,l+1/2}}\sqrt{2}\left|\sqrt{\frac{\alpha^{(1)}}{b^{(1)}}}u^n\right|^2_{\substack{j\\ l+\frac{1}{2}}}h^2
\end{aligned}
$$

$$\leq \lambda \max_{j,l} \left\{ c^{(1)}_{j+\frac{1}{2},l+\frac{1}{2}}, c^{(1)}_{j,l+\frac{1}{2}} \right\} \left(\frac{1}{\sqrt{2}} \left\| \sqrt{\frac{\beta^{(1)}}{a^{(1)}}} p^{n-\frac{1}{2}} \right\|_h^2 + \sqrt{2} \left\| \sqrt{\frac{\alpha^{(1)}}{b^{(1)}}} u^n \right\|_h^2 \right)$$

For the second term we get analogously

$$\Delta t \left| \left\langle \alpha^{(2)} v^n, D_{-y} \left(\beta^{(2)} p^{n-\frac{1}{2}} \right) \right\rangle_h \right|$$
$$\leq \lambda \max_{j,l} \left\{ c^{(2)}_{j+\frac{1}{2},l+\frac{1}{2}}, c^{(2)}_{j+\frac{1}{2},l} \right\} \left(\frac{1}{\sqrt{2}} \left\| \sqrt{\frac{\beta^{(2)}}{a^{(2)}}} p^{n-\frac{1}{2}} \right\|_h^2 + \sqrt{2} \left\| \sqrt{\frac{\alpha^{(2)}}{b^{(2)}}} v^n \right\|_h^2 \right).$$

We thus see that if (18) holds, then

$$\left| \Delta t \left\langle \alpha^{(1)} u^n, D_{-x} \left(\beta^{(1)} p^{n-\frac{1}{2}} \right) \right\rangle_h + \Delta t \left\langle \alpha^{(2)} v^n, D_{-y} \left(\beta^{(2)} p^{n-\frac{1}{2}} \right) \right\rangle_h \right| \leq$$
$$(1-\delta) \left(\left\| \sqrt{\frac{\beta^{(1)}}{a^{(1)}}} p^{n-\frac{1}{2}} \right\|_h^2 + \left\| \sqrt{\frac{\alpha^{(1)}}{b^{(1)}}} u^n \right\|_h^2 + \left\| \sqrt{\frac{\alpha^{(2)}}{b^{(2)}}} v^n \right\|_h^2 \right)$$

and the estimate (25) follows. □

With this we are ready to prove Theorem 3.1.

Theorem 3.1. Let

$$C_1 = \min_{\Omega} \left\{ \frac{\beta^{(1)}}{a^{(1)}}, \frac{\alpha^{(1)}}{b^{(1)}}, \frac{\alpha^{(2)}}{b^{(2)}} \right\},$$
$$C_2 = \max_{\Omega} \left\{ \frac{\beta^{(1)}}{a^{(1)}}, \frac{\alpha^{(1)}}{b^{(1)}}, \frac{\alpha^{(2)}}{b^{(2)}} \right\},$$

then

$$\begin{aligned} \|p^{n-1/2}\|_h^2 + \|u^n\|_h^2 + \|v^n\|_h^2 &\leq \frac{1}{C_1} N_h(p^{n-1/2}, u^n, v^n) \\ &\leq \frac{1}{C_1 \delta} E_h(p^{n-1/2}, u^n, v^n) \\ &= \frac{1}{C_1 \delta} E_h(p^{-1/2}, u^0, v^0) \\ &\leq \frac{2-\delta}{\delta} \frac{1}{C_1} N_h(p^{-1/2}, u^0, v^0) \\ &\leq \frac{2-\delta}{\delta} \frac{C_2}{C_1} \left(\|p^{-1/2}\|_h^2 + \|u^0\|_h^2 + \|v^0\|_h^2 \right). \end{aligned}$$

□

4 Reconciling consistency and stability

To construct a time-stable modification of the coefficients in (9) along the boundary we use as starting point the discretization (11–13). The aim is to modify the coefficients such that the consistency conditions in Table 1 are satisfied at the same time as the stability requirements in Theorem 3.1.

The major restriction that the divergence form discretization (11–13) introduces, compared to the update formula in (9), is that the coefficients on

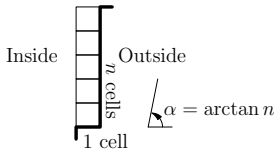

Figure 4: The discretization considered in Theorem 4.1. The p values are centered on the cells shown, with u and v on the edges.

neighbouring stencils couple. This means we have to solve a system of consistency equations on the boundary. As we shall see this system of equations only has a solution for the angles $\alpha = \arctan 1/n$ or $\alpha = \arctan n$, when $n \in \mathbb{Z}$.

To see how we obtain a time-stable modification of the coefficients, consider the divergence form equation given by

$$\begin{aligned} p_t &= a(\partial_x(\alpha_1 u) + \partial_y(\alpha_2 v)), \\ u_t &= b p_x, \\ v_t &= b p_y, \end{aligned}$$

$\alpha_i = \alpha_i(x, y)$, $i = 1, 2$. We discretize this as

$$\begin{aligned} p^{n+\frac{1}{2}}_{j+\frac{1}{2},l+\frac{1}{2}} &= p^{n-\frac{1}{2}}_{j+\frac{1}{2},l+\frac{1}{2}} + \Delta t a_{j+\frac{1}{2},l+\frac{1}{2}} \\ &\quad \times \left(D_{+x}\left(\alpha^{(1)}_{j,l+\frac{1}{2}} u^n_{j,l+\frac{1}{2}} \right) + D_{+y}\left(\alpha^{(2)}_{j+\frac{1}{2},l} v^n_{j+\frac{1}{2},l} \right) \right), \end{aligned} \tag{27}$$

$$u^{n+1}_{j,l+\frac{1}{2}} = u^n_{j,l+\frac{1}{2}} + \Delta t b_{j,l+\frac{1}{2}} D_{-x} p^{n+\frac{1}{2}}_{j+\frac{1}{2},l+\frac{1}{2}}, \tag{28}$$

$$v^{n+1}_{j+\frac{1}{2},l} = v^n_{j+\frac{1}{2},l} + \Delta t b_{j+\frac{1}{2},l} D_{-y} p^{n+\frac{1}{2}}_{j+\frac{1}{2},l+\frac{1}{2}}. \tag{29}$$

which is a special case of (11–13), for which (17) is always satisfied. If we can modify $\alpha^{(1)}$ and $\alpha^{(2)}$ such that the scheme reduces to the usual system (4–6) in the inner domain, while at the same time it satisfies the consistency conditions in Table 1 along the inner boundary, we get a time-stable consistent method. Note that we obtain the time-stability by construction, as this discretization satisfies the conditions in Theorem 3.1.

Theorem 4.1. *Assume the discretization (27–29) with $\alpha^{(1)} = \alpha^{(2)} = 1$ away from the (inner) boundary. Let the angle of the boundary relative to the x-axis be given by $\alpha = \arctan n$, $n \in \mathbb{N}^+$, giving the discretization shown in Fig. 4. Denote the coordinate in the center bottom corner cell by $(x_{j_0+1/2}, y_{l_0+1/2})$. Assume that the coefficient $a_{j+1/2,l+1/2}$ is constant within each group of n cells, i.e., that $a_{j_0+1/2,l_0+1/2+i} = \bar{a}$ for $i = 0, \ldots, n-1$.*

Then the consistency conditions in Table 1 are satisfied if and only if

$$\alpha^{(1)}_{j_0+\frac{1}{2},l_0+i} = \frac{i}{n}, \qquad i = 1, \ldots, n-1, \tag{30}$$

$$\alpha^{(2)}_{j_0+\frac{1}{2},l_0+i} = 1, \qquad i = 1, \ldots, n-1. \tag{31}$$

Proof. By denoting

$$\begin{aligned} a_i^{\mathrm{N}} &= a_{j+\frac{1}{2},l+i-\frac{1}{2}}\alpha^{(2)}_{j+\frac{1}{2},l+i}, \\ a_i^{\mathrm{W}} &= a_{j+\frac{1}{2},l+i-\frac{1}{2}}\alpha^{(1)}_{j,l+i-\frac{1}{2}}, \\ a_i^{\mathrm{S}} &= a_{j+\frac{1}{2},l+i-\frac{1}{2}}\alpha^{(2)}_{j+\frac{1}{2},l+i-1}, \end{aligned}$$

for $i = 1, \ldots, n-1$, the consistency conditions for the cells become

$$\begin{cases} a_n^{\mathrm{W}} \cos\alpha - \left(a_n^{\mathrm{N}} - a_n^{\mathrm{S}}\right) \sin\alpha = 0, \\ a_{n-1}^{\mathrm{W}} \cos\alpha - \left(a_{n-1}^{\mathrm{N}} - a_{n-1}^{\mathrm{S}}\right) \sin\alpha = 0, \\ \qquad \vdots \\ a_2^{\mathrm{W}} \cos\alpha - \left(a_2^{\mathrm{N}} - a_2^{\mathrm{S}}\right) \sin\alpha = 0, \\ a_1^{\mathrm{W}} \cos\alpha - a_1^{\mathrm{N}} \sin\alpha = 0. \end{cases} \tag{32}$$

This is a system of n equations that needs to be solved. Stencils $i = 2$ to n is for when the boundary is to the right (E), and stencil $i = 1$ is when the boundary is to the right and down (SE). See Fig. 2 to recall what E and SE refers to. Since $\alpha^{(1)} = \alpha^{(2)} = 1$ away from the boundary, the conditions we need to impose on the coefficients are

$$a_n^{\mathrm{N}} = \bar{a}, \tag{33}$$

$$a_i^{\mathrm{W}} = \bar{a}, \qquad i = 1, \ldots, n, \tag{34}$$

$$a_{i+1}^{\mathrm{S}} = a_i^{\mathrm{N}} = A_i, \qquad i = 1, \ldots, n-1, \tag{35}$$

where we introduced A_i as the coefficient in between cell i and $i+1$. Thus the system (32) can be written as

$$\begin{cases} \bar{a} - (\bar{a} - A_{n-1})\, n = 0, \\ \bar{a} - (A_{n-1} - A_{n-2})\, n = 0, \\ \qquad \vdots \\ \bar{a} - (A_2 - A_1)\, n = 0, \\ \bar{a} - A_1 n = 0, \end{cases} \tag{36}$$

where we note that the first equation is the sum of the other $n-1$ equations. Thus we get the unique solution

$$A_i = \frac{i}{n}\bar{a}, \qquad i = 1, \ldots, n-1,$$

and hence (30–31) follows. □

Corollary 4.1. *The result in Theorem 4.1 is by symmetry also valid for* $\alpha = \arctan 1/n$ *and* $\alpha = \arctan n$, $n \in \mathbb{Z}$.

Corollary 4.2. *From the system* (36) *we see that if* $\arctan\alpha \neq n$, $n \in \mathbb{N}$, *then the first equation is no longer the sum of the remaining* $n-1$ *equations and the system does not have a solution. Thus we can not obtain a discretization of the form (27–29) that satisfies the consistency conditions if* $\arctan\alpha \neq n$.

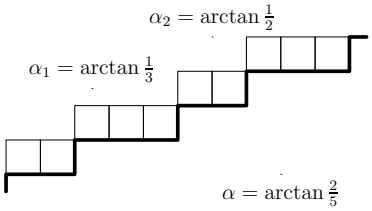

Figure 5: The staircase approximation of the $\alpha = \arctan 2/5$ case is shown as a dark line. Piecewise $1/n$ approximation amounts to setting the angle to $\alpha = \arctan 1/3$ and $\arctan 1/2$ in the consistency conditions for the three and two cells, respectively, that are in a horizontal row.

Remark 4.1. The condition (18) for the modifications (30–31) reduces to the standard CFL condition $c\lambda < 1/\sqrt{2}$ for the Yee-scheme.

Remark 4.2. The $\mathcal{O}(1)$ truncation error in L_∞ on the boundary means we get $\mathcal{O}(\sqrt{h})$ truncation error in L_2, since the number of boundary cells scale as $\mathcal{O}(1/N)$. Stability in L_2 then implies $\mathcal{O}(\sqrt{h})$ convergence. However, in [7] it was shown that under some conditions there is a one order gain in the global error compared to the boundary error. Although our case is not covered by this theory, in the numerical tests in Section 5 this is what is observed, where the convergence rate is $\mathcal{O}(h)$.

4.1 Piecewise and partially modified coefficients

In Theorem 4.1, time-stability was reconciled with $\mathcal{O}(h)$ accuracy for a subset of rational angles. To improve the accuracy for an arbitrary angle while keeping the time-stability of the original Yee scheme, one can approximate the boundary by piecewise $1/n$ angles, as illustrated in Fig. 5. As an example, consider the boundary given by the line with the angle $\alpha = \arctan 2/5$ with respect to the x-axis. The usual staircasing gives a repeated pattern of $1/2$ and $1/3$ cells. Again, this can be seen clearly in Fig. 5. Instead of setting $\alpha = \arctan 2/5$ in the consistency relations, we set either $\alpha = \arctan 1/2$ or $\arctan 1/3$ depending on if the cell is part of a $1/2$ or $1/3$ group of cells.

Effectively, this means that like the Yee scheme we still have $\mathcal{O}(1)$ errors in L_∞, but with a much smaller constant. See e.g. Fig. 17, which shows that the computed field is qualitative much improved.

Hence we see that we can construct a piecewise approximation of an angled boundary by the repeated application of (30). We will refer to this method as *piecewise modification*, or *piecewise Tornberg–Engquist*.

An alternative way to piecewise approximate a non-integer angle is to simply skip the first equation in the system (32). Applying the same conditions (33–35) then gives the coefficients

$$\alpha^{(1)}_{j_0+\frac{1}{2},l_0+i} = \frac{i}{\tan\alpha}, \qquad i = 1,\dots,n-2, \tag{37}$$

$$\alpha^{(1)}_{j_0+\frac{1}{2},l_0+n-1} = 1, \tag{38}$$

$$\alpha^{(2)}_{j_0+\frac{1}{2},l_0+i} = 1, \qquad i = 1,\dots,n-1. \tag{39}$$

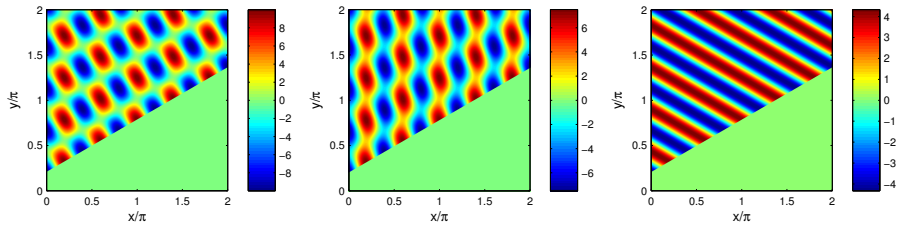

(a) p (b) u (c) v

Figure 6: Exact field used for convergence study.

It has been observed in some cases that the error in the outer most cell, i.e., in this case top cell, is insignificant compared to the rest, making this strategy in modification effective. Eq. (37–39) will be referred to as *partial modification*, or *partial Tornberg–Engquist*. It should be emphasized that both piecewise and partial Tornberg–Engquist modifications are time-stable.

5 Test cases

5.1 Straight boundary

We run the numerical tests on a $[0, 2\pi] \times [0, 2\pi] \subset \mathbb{R}^2$ domain with homogeneous Dirichlet outer boundary conditions for the (u, v) field. The field is set to an exact solution, and the timestepped until $t = 0.3\pi$, when we measure the error in (discrete) L_2 and L_∞ norms. The coefficients are set to $a = b = -1$. To test the modified coefficients we set an internal inclined boundary defined by $y(x) = (x - \bar{x}) \tan \alpha$ so that the inner domain and boundary becomes

$$\Omega = \{(x, y) \subset [0, 2\pi] \times [0, 2\pi] \mid y > (x - \bar{x}) \tan \alpha\},$$
$$\Gamma = \{(x, y) \subset [0, 2\pi] \times [0, 2\pi] \mid y = (x - \bar{x}) \tan \alpha\}.$$

The angle α is relative to the x-axis. When measuring errors we only include an inner subset $\bar{\Omega} \subset \Omega$ of the domain in such a way that the effects from the outer boundary has not yet propagated into the area where we measure. Outside of the discrete L_2-norm defined by (14–16), we also use

$$\|p\|_\infty = \max_{j,l \in \Omega_N^p} |p_{j+1/2,l+1/2}|,$$
$$\|u\|_\infty = \max_{j,l \in \Omega_N^u} |u_{j,l+1/2}|,$$
$$\|v\|_\infty = \max_{j,l \in \Omega_N^v} |v_{j+1/2,l}|.$$

The exact solution for a reflected harmonic wave is used. Let

$$\varphi = e^{i\mathbf{k}_I \cdot \mathbf{x}} + e^{ikx^\star} e^{i\mathbf{k}_R \cdot (\mathbf{x} - \mathbf{x}^\star)}$$

where $\mathbf{k}_I = (k, 0)$, $\mathbf{k}_R = k \cdot (\cos 2\alpha, \sin 2\alpha)$, $k = \omega/c$ and $\mathbf{x}^\star = (x^\star, y^\star)$ is any

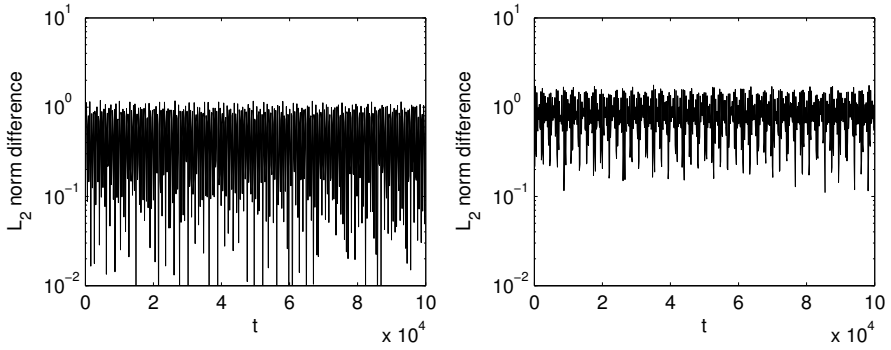

(a) $\|p^{n-1/2}\|_h$ (b) $\|\mathbf{u}^n\|_h$

Figure 7: Numerical stability test of the piecewise modifications by initializing with random data to excite all frequencies. The angle of the boundary is $\alpha = \arctan 2/5$ and is divided into sections with $\alpha = \arctan 1/2$ and $\alpha = \arctan 1/3$. CFL is 0.3.

point on the boundary. Then the fields given by

$$p(x, y, t) = \frac{1}{b}\Re(\partial_t \varphi e^{-i\omega t}), \tag{40}$$

$$\mathbf{u}(x, y, t) = \Re(\nabla \varphi e^{-i\omega t}), \tag{41}$$

satisfy both (1–2) and the boundary conditions (7–8). These are visualized in Fig. 6 for $k = 5$.

We observe the stability of the piecewise modification of coefficients in Fig. 7, where the modification is according to Theorem 4.1. This verifies the analysis, as we appear to have time-stability with the field bounded independently of the time t.

In Fig. 8–10 we can observe the resulting fields when time stepping with standard Yee, Tornberg–Engquist modified coefficients and piecewise modifications for the angle $\arctan 2/5$. In both cases where the coefficients are modified we see a clear improvement in the quality of the solution. In the standard Yee case we clearly see the $\mathcal{O}(1/h)$ truncation error being generated at the boundary and then being propagated into the domain.

With regards to accuracy we plot the convergence in Fig. 11–12 at $t = 0.3\pi$. We see that the unmodified Yee scheme behaves as $\mathcal{O}(\sqrt{h})$ in the discrete L_2 norm and $\mathcal{O}(1)$ in L_∞. Both type of modifications, standard Tornberg–Engquist and piecewise modifications, give a clear $\mathcal{O}(h)$ convergence in both L_2 and L_∞ for $\alpha = \arctan 1/3$. The most interesting case is when $\alpha = \arctan 2/5$ in Fig. 12. We see a marked improvement in the point wise error for piecewise modifications compared to the traditional Yee scheme, and a solid $\mathcal{O}(h)$ convergence in L_2. Partial modification according to (37–39) gives, in this case, the same convergence line as Tornberg–Engquist. This indicates that the error is not evenly distributed, with most of it occurring in and near the corner cells (bottom in Fig. 4), and very little in the cells where the consistency condition is violated.

Fig. 12b might be source of concern, since it appears we do not have convergence. However running the test for grid resolutions typically used in applica-

tions, which are in usually in the span of 10–90 points per wavelength, we get Fig. 13, where we clearly see first order convergence in L_∞. The errors generated by the staircasing has a broad spectrum, seen in Fig. 14, and modifying the coefficients removes most of the high frequency errors.

5.2 Cylinder

The second test case is when we replace the straight inclined inner boundary with a circular cylinder at $(x_c, y_c) = (\pi, \pi)$ with radius $R = 4\pi/15$. Again we compare against the exact solution for the scattering of a harmonic wave, which in polar coordinates (r, θ) is given by

$$\varphi^{\text{inc}}(r,\theta) = e^{ikr\cos\theta} = J_0(kr) + \sum_{n=1}^{\infty} 2(i)^n J_n(kr)\cos n\theta,$$
$$\varphi^{\text{ref}}(r,\theta) = \sum_{n=0}^{\infty} M_n H_n^{(1)}(kr)\cos n\theta$$

together with (40–41). The expansion coefficients for the reflected field are determined by the boundary conditions, giving

$$M_0 = -\frac{J_0'(kR)}{H_0^{(1)'}(kR)},$$
$$M_n = -\frac{2(i)^n J_n'(kR)}{H_n^{(1)'}(kR)}$$

These include Bessel functions J_n as well as Hankel functions of first kind $H_n^{(1)}$.

The domain is

$$\Omega = \{(x,y) \subset [0,2\pi] \times [0,2\pi] \mid (x-x_c)^2 + (y-y_c)^2 \geq 1\}$$

and we measure the error in the subset $\bar{\Omega} = ([\pi/2, 3\pi/2] \times [\pi/2, 3\pi/2]) \cap \Omega$ at time $t = 0.3\pi$, meaning that the effects from the outer boundary is cropped.

Close-ups of the time-evolved field is shown in Fig. 17, where we see a drastic difference in quality compared to standard Yee. Convergence results are shown in Fig. 15, where we see a clear improvement, especially in L_2. The convergence line in L_∞ flattens out for finer resolutions similarly as for the straight line case. However, in Fig. 16 we still observe convergence for grid spacings typically employed in applications. N denotes the number of grid points along each axis. It should be noted that Dey–Mittra style locally conformal methods suffer from a similar loss of convergence at small grid spacings, albeit for completely different reasons [17].

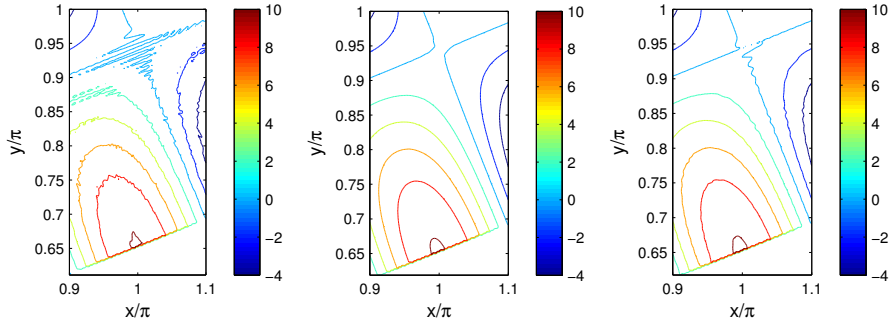

(a) Standard Yee (b) Tornberg–Engquist (c) Piecewise modified

Figure 8: close-ups of the computed p field for the angle $\arctan 2/5$ of the inner boundary. The grid size is $n = 900$ and the field is shown at $t = 0.3\pi$.

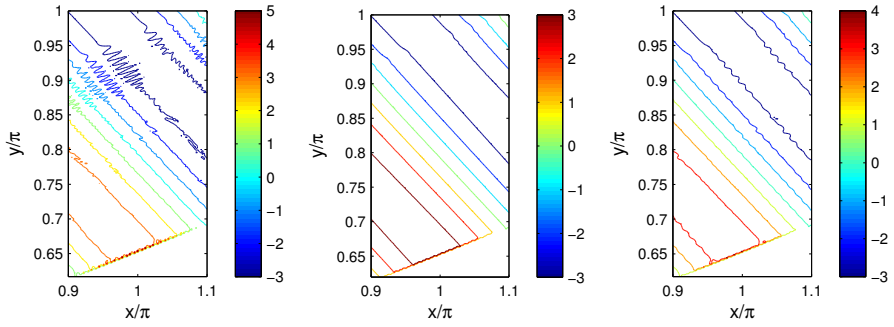

(a) Standard Yee (b) Tornberg–Engquist (c) Piecewise modified

Figure 9: close-ups of the computed u field for the angle $\arctan 2/5$ of the inner boundary. The grid size is $n = 900$ and the field is shown at $t = 0.3\pi$.

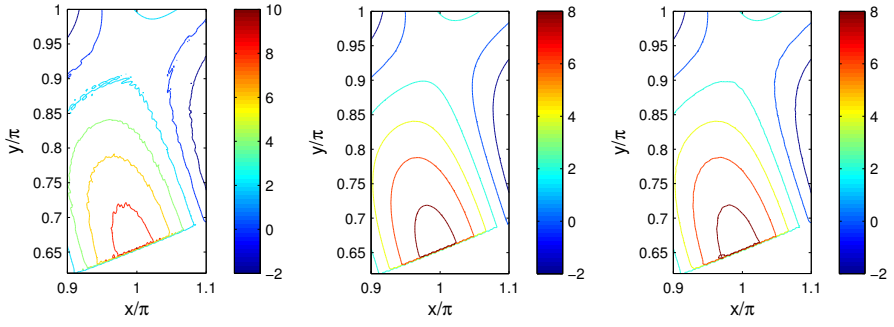

(a) Standard Yee (b) Tornberg–Engquist (c) Piecewise modified

Figure 10: close-ups of the computed v field for the angle $\arctan 2/5$ of the inner boundary. The grid size is $n = 900$ and the field is shown at $t = 0.3\pi$.

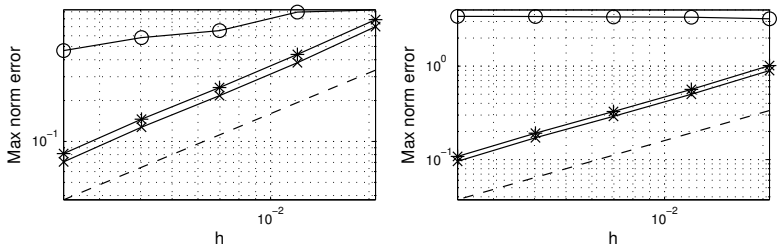

(a) p field (b) $\mathbf{u}$ field

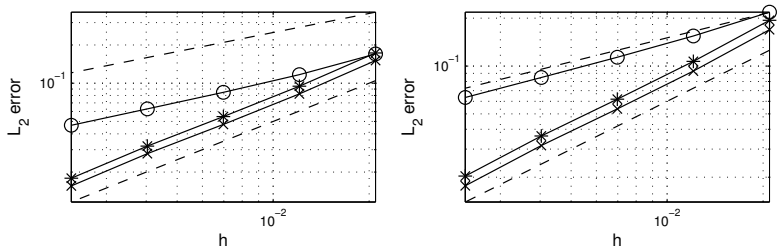

(c) p field (d) $\mathbf{u}$ field

Figure 11: Convergence study in L_∞ and L_2 norm for the angle $\alpha = \arctan 1/3$. ($\circ$) is standard FDTD, ($\times$) is Tornberg–Engquist and ($\star$) is piecewise modification. Dashed lines indicate slope of $1/2$ and 1.

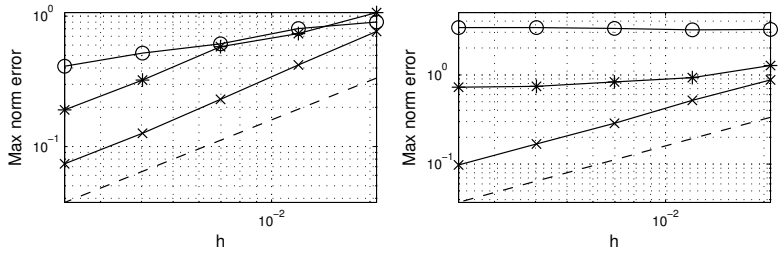

(a) p field (b) $\mathbf{u}$ field

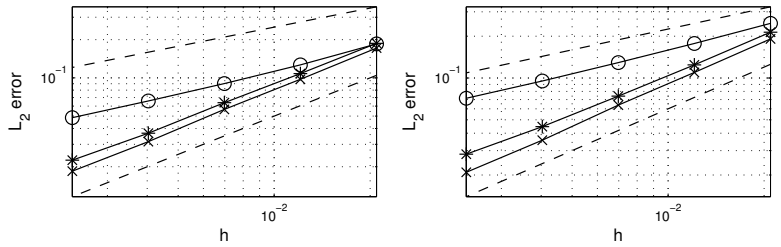

(c) p field (d) $\mathbf{u}$ field

Figure 12: Convergence study in L_∞ and L_2 norm for the angle $\alpha = \arctan 2/5$. ($\circ$) is standard FDTD, ($\times$) is Tornberg–Engquist and ($\star$) is piecewise modification. Dashed lines indicate slope of $1/2$ and 1. The error for partial modification according to (37–39) is also computed and gives the same convergence line as Tornberg–Engquist.

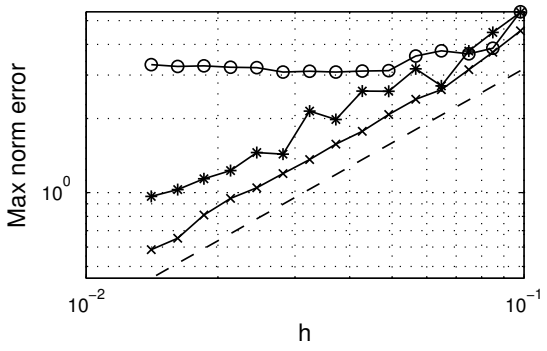

Figure 13: The same setup as Fig. 12b but restricted to $h \in [10^{-2}, 10^{-1}]$, which corresponds to approximately 10–100 points per wave length. This gives the convergence of the velocity field $\mathbf{u}$ for grid resolutions typical in applications. The wave number is $k = 5$ and the angle is $\alpha = \arctan 2/5$. ($\circ$) is standard FDTD, ($\times$) is Tornberg–Engquist and ($\star$) is piecewise modification. The dashed line indicates slope of 1.

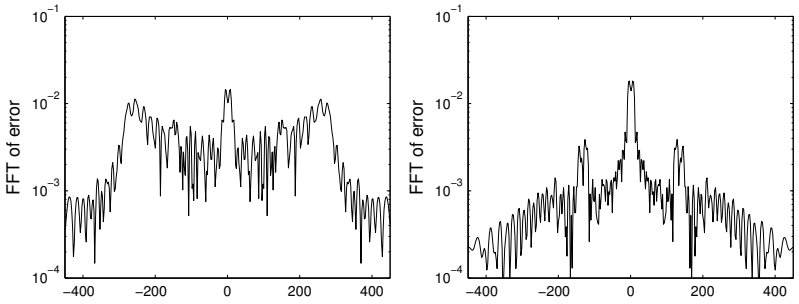

(a) Standard Yee (b) Piecewise modified

Figure 14: FFT of the error along $x = \pi$ in the middle of the domain. A sharp reduction of high frequency errors for modified coefficients is observed.

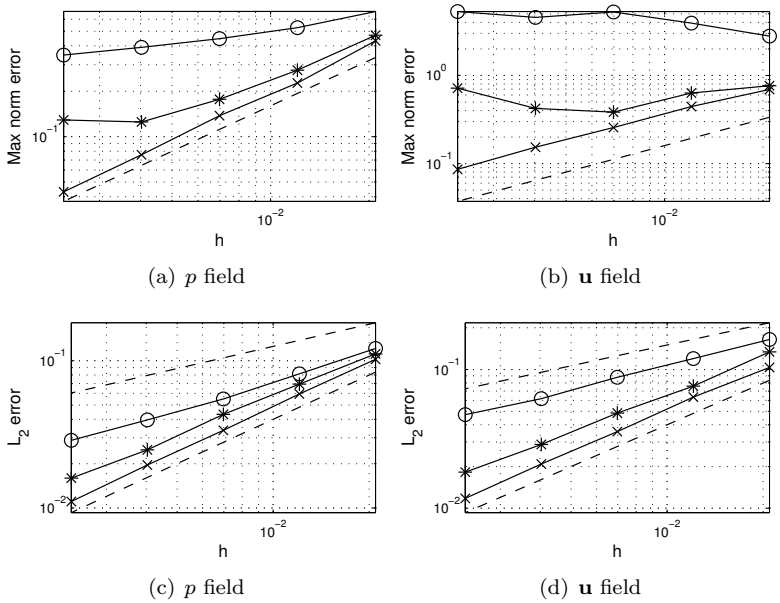

(a) p field (b) $\mathbf{u}$ field

(c) p field (d) $\mathbf{u}$ field

Figure 15: Convergence study in L_∞ and L_2 norm for the cylinder case. ($\circ$) is standard FDTD, ($\times$) is Tornberg–Engquist and ($\star$) is piecewise modification. Dashed lines indicate slope of 1/2 and 1.

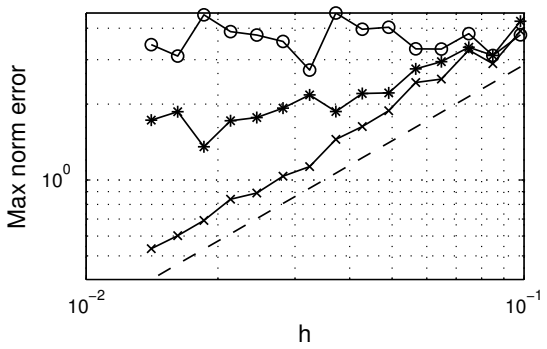

Figure 16: The same setup as Fig. 15b but restricted to $h \in [10^{-2}, 10^{-1}]$, corresponding to approximately 10–100 points per wave length. This gives the convergence of the velocity field $\mathbf{u}$ for grid resolutions typical in applications. ($\circ$) is standard FDTD, ($\times$) is Tornberg–Engquist and ($\star$) is piecewise modification. The dashed line indicates slope of 1.

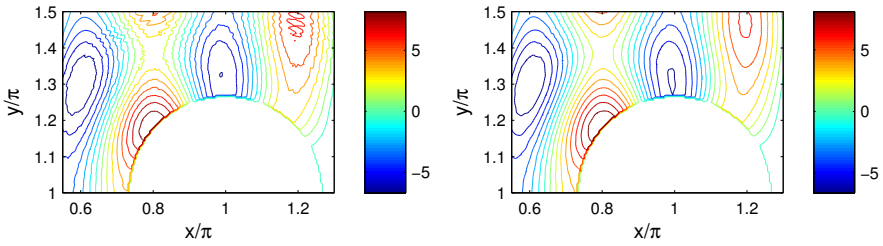

(a) p field, standard Yee

(b) p field, piecewise modified

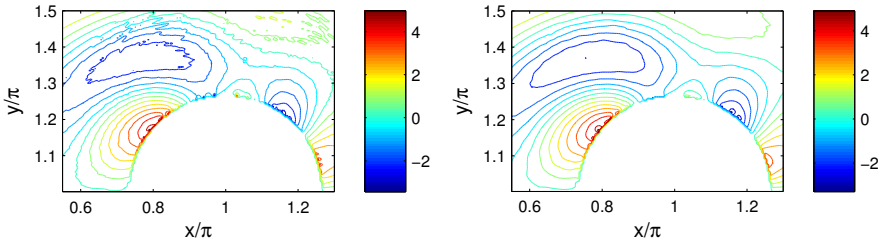

(c) u field, standard Yee

(d) u field, piecewise modified

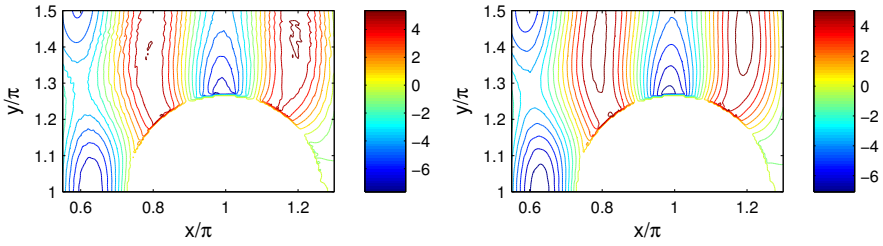

(e) v field, standard Yee

(f) v field, piecewise modified

Figure 17: Close-ups of the computed v field. The grid size is $N = 400$ and the field is shown at $t = 0.3\pi$.

6 Conclusions

We have extended the consistent boundary treatment in [28] of the Yee scheme for oblique boundaries in two dimensions, such that we obtain time-stability, i.e., strict energy conservation. This is done by modifying the coefficients of the update stencil near the boundary without changing the simple structure of the Yee scheme, including the optimal CFL condition. Stability has been proved using the energy method. Both stability and accuracy is demonstrated with numerical tests. Some, but not all of the properties established here extend to three dimensions and material interfaces. This will be further studied and discussed in a subsequent publication.

References

[1] A.C. Cangellaris and D.B. Wright. Analysis of the numerical error caused by the stair-stepped approximation of a conducting boundary in FDTD simulations of electromagnetic phenomena. *IEEE T. Antenn. Propag.*, 39(10):1518 –1525, oct. 1991.

[2] Mark H. Carpenter, David Gottlieb, and Saul Abarbanel. Time-stable boundary conditions for finite-difference schemes solving hyperbolic systems: Methodology and application to high-order compact schemes. *J. Comput. Phys.*, 111(2):220 – 236, 1994.

[3] S. Dey and R. Mittra. A locally conformal finite-difference time-domain (FDTD) algorithm for modeling three-dimensional perfectly conducting objects. *IEEE Microw. Guided. W.*, 7(9):273 –275, sep. 1997.

[4] S. Dey and R. Mittra. A modified locally conformal finite-difference time-domain algorithm for modeling three-dimensional perfectly conducting objects. *Microw. Opt. Technol. Lett.*, 17(6):349–352, 1998.

[5] A. Ditkowski, K. Dridi, and J. S. Hesthaven. Convergent cartesian grid methods for Maxwell's equations in complex geometries. *J. Comput. Phys.*, 170(1):39 – 80, 2001.

[6] David Gottlieb, Bertil Gustafsson, Pelle Olsson, and Bo Strand. On the superconvergence of galerkin methods for hyperbolic IBVP. *SIAM J. Numer. Anal.*, 33(5):pp. 1778–1796, 1996.

[7] Bertil Gustafsson. The convergence rate for difference approximations to mixed initial boundary value problems. *Math. Comp.*, 29(130):pp. 396–406, 1975.

[8] Bertil Gustafsson. *High Order Difference Methods for Time Dependent PDE*. Springer, 2008.

[9] Bertil Gustafsson, Heinz-Otto Kreiss, and Arne Sundström. Stability theory of difference approximations for mixed initial boundary value problems. ii. *Math. Comp.*, 26(119):pp. 649–686, 1972.

[10] Yang Hao and C.J. Railton. Analyzing electromagnetic structures with curved boundaries on Cartesian FDTD meshes. *IEEE T. Microw. Theory.*, 46(1):82 –88, jan. 1998.

[11] J.S. Hesthaven. High-order accurate methods in time-domain computational electromagnetics: A review. *Adv. Imag. Electron Phys.*, 127:59 – 123, 2003.

[12] R. Holland. Pitfalls of staircase meshing. *IEEE T. Electromagn. C.*, 35(4):434 –439, nov. 1993.

[13] T.G. Jurgens and A. Taflove. Three-dimensional contour FDTD modeling of scattering from single and multiple bodies. *IEEE T. Antenn. Propag.*, 41(12):1703 –1708, December 1993.

[14] T.G. Jurgens, A. Taflove, K. Umashankar, and T.G. Moore. Finite-difference time-domain modeling of curved surfaces [EM scattering]. *IEEE T. Antenn. Propag.*, 40(4):357 –366, apr. 1992.

[15] Ken Mattsson. Boundary procedures for summation-by-parts operators. *J. Sci. Comput.*, 18:133–153, February 2003.

[16] A. Monorchio and R. Mittra. A hybrid finite-element finite-difference time-domain (FE/FDTD) technique for solving complex electromagnetic problems. *IEEE Microw. Guided. W.*, 8(2):93 –95, feb. 1998.

[17] C. Nieter, John R. Cary, Gregory R. Werner, David N. Smithe, and Peter H. Stoltz. Application of dey-mittra conformal boundary algorithm to 3d electromagnetic modeling. *J. Comput. Phys.*, 228:7902–7916, November 2009.

[18] Jan Nordström, Karl Forsberg, Carl Adamsson, and Peter Eliasson. Finite volume methods, unstructured meshes and strict stability for hyperbolic problems. *Appl. Numer. Math.*, 45(4):453 – 473, 2003.

[19] C.J. Railton and I.J. Craddock. Stabilised CPFDTD algorithm for the analysis of arbitrary 3D PEC structures. *IEE Proc. Microwaves Antennas Propag.*, 143(5):367 –372, oct. 1996.

[20] C.J. Railton and J.B. Schneider. An analytical and numerical analysis of several locally conformal FDTD schemes. *IEEE T. Microw. Theory.*, 47(1):56 –66, jan. 1999.

[21] Thomas Rylander and Anders Bondeson. Stable FEM-FDTD hybrid method for Maxwell's equations. *Comput. Phys. Commun.*, 125(1-3):75 – 82, 2000.

[22] J. S. Shang. High-order compact-difference schemes for time-dependent Maxwell equations. *J. Comput. Phys.*, 153(2):312 – 333, 1999.

[23] Julius G. Tolan and John B. Schneider. Locally conformal method for acoustic finite-difference time-domain modeling of rigid surfaces. *J. Acoust. Soc. Am.*, 114(5):2575–2581, 2003.

[24] A.-K. Tornberg. Regularization techniques for singular source terms in differential equations. In *A. Laptev, editor, European Congress of Mathematics (ECM), Stockholm, Sweden, June 27–July 2 2004*. Zurich: European Mathematical Society, 2005.

[25] Anna-Karin Tornberg and Björn Engquist. Regularization techniques for numerical approximation of PDEs with singularities. *J. Sci. Comput.*, 19:527–552, December 2003.

[26] Anna-Karin Tornberg and Björn Engquist. Numerical approximations of singular source terms in differential equations. *J. Comput. Phys.*, 200:462–488, November 2004.

[27] Anna-Karin Tornberg and Björn Engquist. Regularization for accurate numerical wave propagation in discontinuous media. *Methods Appl. Anal.*, 13:247–274, 2006.

[28] Anna-Karin Tornberg and Björn Engquist. Consistent boundary conditions for the Yee scheme. *J. Comput. Phys.*, 227(14):6922–6943, 2008.

[29] Anna-Karin Tornberg, Björn Engquist, Bertil Gustafsson, and Per Wahlund. A new type of boundary treatment for wave propagation. *BIT*, 46:145–170(26), November 2006.

[30] Lloyd N. Trefethen. Stability of finite-difference models containing two boundaries or interfaces. *Math. Comp.*, 45(172):pp. 279–300, 1985.

[31] Eli Turkel. Progress in computational physics. *Comput. & Fluids*, 11(2):121 – 144, 1983.

[32] Ruey-Beei Wu and T. Itoh. Hybrid finite-difference time-domain modeling of curved surfaces using tetrahedral edge elements. *IEEE T. Antenn. Propag.*, 45(8):1302 –1309, aug. 1997.

[33] K. S. Yee. Numerical solution of initial boundary value problems involving Maxwell's equations in isotropic media. *IEEE T. Antenn. Propag.*, 14:302–307, 1966.

[34] J.L. Young, D. Gaitonde, and J.S. Shang. Toward the construction of a fourth-order difference scheme for transient em wave simulation: staggered grid approach. *IEEE T. Antenn. Propag.*, 45(11):1573 –1580, nov 1997.

[35] W. Yu and R. Mittra. A conformal FDTD algorithm for modeling perfectly conducting objects with curve-shaped surfaces and edges. *Microw. Opt. Technol. Lett.*, 27(2):136–138, 2000.

[36] I. Zagorodnov, R. Schuhmann, and T. Weiland. A uniformly stable conformal FDTD-method in cartesian grids. *Int. J. Numer. Model.*, 16(2):127–141, 2003.

[37] Igor Zagorodnov, Rolf Schuhmann, and Thomas Weiland. Conformal FDTD-methods to avoid time step reduction with and without cell enlargement. *J. Comput. Phys.*, 225(2):1493–1507, 2007.